Dynamics of Microsphere Suspensions Probed by High-Frequency Dynamic Ultrasound Scattering

Mariko Kohyama, Tomohisa Norisuye,* and Qui Tran-Cong-Miyata

Department of Macromolecular Science and Engineering, Graduate School of Science & Technology, Kyoto Institute of Technology Matsugasaki, Sakyo-ku, Kyoto 606-8585, Japan

Received August 28, 2008; Revised Manuscript Received December 7, 2008

ABSTRACT: The sedimentation velocity and its fluctuations were investigated for polystyrene microspheres with the diameter 3.6−32 μm by high-frequency dynamic ultrasound scattering. A longitudinal broadband transducer centered at the nominal frequency 20 MHz was employed to probe the particle dynamics along the directions parallel and perpendicular to the sedimentation direction in highly turbid solutions. For the former case, the average sedimentation velocity and its variance were obtained since the direction of the scattering vector coincides with that of the particle displacement. Subsequently, the velocities were calculated to estimate the particle diameters. On the other hand, the velocity fluctuations can be solely determined when the wave propagation direction is normal to the gravity because the average displacement is zero. The velocity fluctuations were evaluated as a function of the sample position, and it was found that the significant decrease in the velocity fluctuations near the two cell walls was observed. The resonance scattering could have an additional role, exclusive for the large particles. Analysis on particle sizing was also attempted from the measurements of the horizontal velocity fluctuations.

Introduction

There has been great attention to polymer microspheres because of the versatile applications, such as inks, cosmetics, fillers, spacers, catalytic support, and standard calibration. Various techniques, such as optical and electron microscopes, atomic force microscopy, electrophoresis, static/dynamic light scattering, and so on, are available nowadays to evaluate the size and its distribution.[1] In-situ monitoring the particle suspension is sometimes required to be observed as is. This is particularly important if the systematic quality control is required for the subsequent manufacture process. Particle image velocimetry (PIV),[2] ultrasound Doppler velocimetry (UDV),[3] or dynamic light scattering (DLS)[4] is one of the most promising techniques to fulfill the requirement. Among them, DLS based on a correlation spectroscopy technique allows one to investigate complex dynamics of polymer solutions[5−8] and gels[9−11] at a molecular level beyond the diffraction limit. More recently, DLS was employed to detect oligomers[12] or low molecular weight species[13,14] which exhibited fairly rapid relaxation processes. On the contrary, since visible light is not able to pass though opaque media, the samples should be optically transparent by dilution or sufficiently thin to allow transmission of the light source.

An ultrasound-based new technique called dynamic sound scattering (DSS) or diffusing acoustic wave spectroscopy (DAWS) may be useful to investigate the dynamics of suspensions. DSS and DAWS were proposed by Page and co-workers[15] and employed to investigate complex fluid motion, which was generally difficult to investigate by conventional UDV. Fluidized particles motion against gravity[16] or neutrally buoyant suspensions in the Couette geometry[17−19] is an example. These experiments were carried out by longitudinal ultrasound waves with the frequency several hundred kilohertz to several megahertz in order to detect the dynamics of the particles with the size ranging from millimeters to sub-millimeters. On the contrary, the detectable particle size was still far from the microscopic length scale. As the spatial resolution was improved upon increasing frequency, DSS was further developed with the higher frequency source[20] where the employed wavelength was 10 times shorter than the previous works by Page et al.[16,21] This enables detection of the smaller particles on the order of several micrometers or even smaller. However, it becomes more difficult to obtain good signals because of the serious attenuation at high frequencies. Therefore, 20 MHz ultrasound may be a good compromise between the resolution and the data quality.

The principle of DSS is more or less similar to conventional DLS that is often employed to determine the characteristic time and hydrodynamic radius of submicron particles. However, high-frequency DSS has further advantages to be utilized in hydrodynamic characterization. For example, it can be used in (1) highly turbid solutions where the no signal from transmitted light is detected and (2) dynamic analysis of particles having relatively large size, which is generally inaccessible by conventional DLS without a priori knowledge about the intramolecular form factor.[22,23] Moreover, (3) accessible information is not only the pulse strength (or scattering intensity) but also the phase of the scattering waves. This is due to the fact that ultrasound velocity is very much smaller than that of visible light, although traveling of sound is still much faster than the particle motion. Therefore, the complete waveform including the sample position information can be captured by a high-speed digitizer with a sufficient physical RAM, which becomes close and personal more recently.

When an ultrasonic pulse is irradiated onto a suspension of microspheres whose particle size is comparable with the wavelength of ultrasound, scattering is observed. The scattered amplitude depends on the density or the adiabatic compressibility differences between the particles and the surrounding medium.[24,25] The scattering intensities generally fluctuate with time due to the particle dynamics such as diffusion, sedimentation, and/or interparticle collision. Although the frequency actually shifts due to the Doppler effect, the dynamics can be still probed by the field fluctuations within the framework of quasi-elastic scattering since the energy shift due to the particle motion (∼Hz) is much smaller than the source frequency (∼20 MHz). The characteristic time is determined by a traveling time of the particles passing through a probing distance on the order of inverse of q. In the case of DSS at high frequency as studied

* To whom correspondence should be addressed. E-mail: nori@kit.jp.

10.1021/ma801949y CCC: $40.75
Published on Web 01/13/2009

Table 1. Characteristics of the Particle Size d Obtained by SEM, the Coefficient of Variation CV, Density ρ, the Terminal Velocity V_0, the Sedimentation Time T_{sed}, and the Recording Time T_{meas}

d (μm)	CV	ρ (g/cm^3)	V_0 (mm/s)	T_{sed} (min)	T_{meas} (min)
3.6	0.07	1.183	0.0013	175	3.8
5.5	0.05	1.189	0.0031	56	1.7
18	0.039	1.189	0.0336	4	1
32	0.11	1.177	0.0995	2	0.7

here, the characteristic time of the micrometer size particles was found to be on the order of milliseconds to seconds depending on the sample characteristics. In this study, DSS is utilized for quantitative evaluation of the sedimentation velocity, thereby determining the particle size. The position dependence of the velocity fluctuations is also discussed.

Experimental Section

Samples. Standard latex microspheres were supplied by courtesy of Sekisui Chemical Co. Ltd. The particles were dispersed in an aqueous solution containing 0.2% sodium dodecyl sulfate (SDS) to obtain a suspension with desired concentrations in range $0.5 < C < 2.9$ wt %, followed by a brief immersion in a low-power ultrasonic bath prior to DSS experiments in order to avoid aggregation. Note that the microspheres were made from *p*-divinylbenzene according to a separate Fourier transform infrared spectroscopy measurement. Disposal polystyrene rectangular vessels with the dimension 10 × 10 × 40 mm and the wall thickness 1 mm were used as the sample cells. The maximum scattering path was 10 mm for all the experiments. For the horizontal setup addressed below, the sample was illuminated at 15 mm from the bottom. For the vertical setup, the sedimentation time T_{sed} for the 10 mm path was visually confirmed. The ultrasonic transducer and the cell container were carefully aligned by using a custom-made stainless stage prior to the DSS experiments. DSS experiments were carried out after gentle shaking and waiting at least 20 s in order to avoid formation of air bubbles. The DSS measurements were repeated at least 10 times in order to gain the better statistics. SEM micrographs (Hitachi S-3000N) were also taken to verify the particle size and its distribution. A 25 mL Gay-Lussac pycnometer was used to measure the densities to three places of decimals. The particle size d, the coefficient of variation CV, density ρ, the terminal velocity V_0, the sedimentation time T_{sed}, and the recording time T_{meas} are summarized in Table 1. The particle Reynolds number was extremely small ($Re_p \sim 10^{-3}$) so that the effect of inertia was negligible. All the experiments were performed at 20.0 ± 0.05 °C.

Apparatus. Negative impulse emitted from a pulser/receiver (Olympus, model 5800PR) was transferred to a 20 MHz longitudinal plane wave transducer (Olympus, model V317, bandwidth 40%, 0.25 in. diameter) immersed in a water bath to generate broadband ultrasound pulses. The reflected or scattered ultrasound wave was received by the same transducer for the backscattering experiments. The sample-to-detector distance was 11 mm. To measure the attenuation coefficient, α, and the phase velocity, v_p, in the transmission experiments, two transducers were faced to emit and receive the signals.[27] The obtained signals were then amplified by the receiver, followed by successive recording with a 14-bit high-speed digitizer (GaGe, Compuscope CS14200) at the sampling rate 200 MS/s. A digital delay (Stanford, DG535) was employed to control the acquisition timing of the input and output signals by taking account of the traveling time of sound in water. All the digital equipments were synchronized with a 10 MHz reference clock in order to avoid the phase jittering. The pulse repetition rate and the number of sampling points for successive pulse were tunable. For example, 3000 points of a propagation wave were recorded every 1 ms until the total recording number reached 10^4. The magnitude of the scattering vector q is given by

$$q = \frac{4\pi}{\lambda}\sin\left(\frac{\theta}{2}\right) = \frac{4\pi f}{v_p}\sin\left(\frac{\theta}{2}\right) \quad (1)$$

where f and θ are the central frequency and scattering angle, respectively. In the case of ultrasound pulse centered at 20 MHz, λ and q are respectively 71 μm and 0.177 μm^{-1} for the microsphere ($d = 3.6$ μm) at $C = 1$ wt %. The appropriate v_p evaluated by the transmission experiments was used to estimate q for each data.

Scheme 1. Illustrations of the (a) Vertical and (b) Horizontal Setups with the Corresponding Field Amplitude; (c) Field Amplitude Was Repetitively Recorded To Construct a Matrix

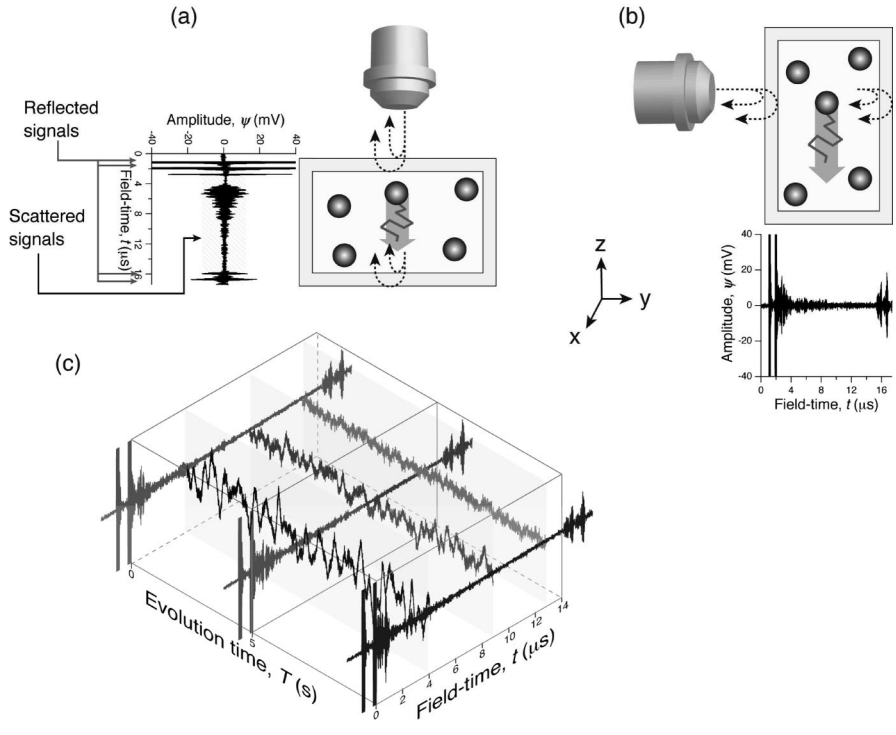

Scheme 2. Illustrations of the Scattering Vector, q[a]

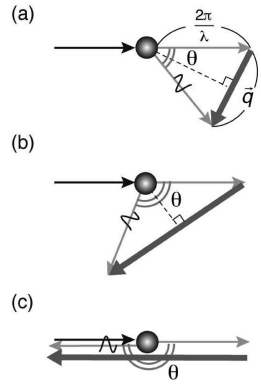

[a] In the case of the back scattering geometry, q coincides with the direction of the beam emission.

Results and Discussion

When ultrasound is emitted from a radiator as illustrated in Scheme 1a, it passes through a sample cell containing a microsphere suspension. In a backscattering geometry, the same transducer receives the scattering signals, which are generally observed as temporal amplitude ψ between the reflected signals from the two stationary walls on the field-time axis, t. Here the field time is defined as the propagation time of ultrasound. In the scheme, ψ was vertically truncated around ± 40 mV for the sake of visibility of the weak scattering signals. When such a waveform is repetitively captured at a constant time interval ΔT called pulse repetition time, ψ fluctuates with the evolution time T, providing the information about the particle position as functions of both t and T. The time-fluctuating signals $\psi(t,T)$ are subsequently processed to construct a time-correlation function which allows us to achieve quantitative evaluation of the characteristic time τ. While both setups in Scheme 1a,b provide certain sedimentation dynamics, the accessible information is fairly different depending on the beam direction as explained below.

As represented in Scheme 2, the magnitude of the scattering vector q corresponding to the difference of the vector components between the incident and scattered waves becomes larger with increasing the scattering angle θ. In the case of backscattering geometry, $\theta = 180°$, the direction of q coincides with that of the beam emission. Therefore, the sedimentation dynamics can be probed by DSS along the z-axis (parallel to the sedimentation direction) as shown in Scheme 1a. On the other hand, when ultrasound is emitted normal to the gravity as shown in Scheme 1b, the average velocity for sedimentation is never accessible because the average displacement along the y-axis is zero. Nevertheless, time-dependent components along the y-axis can be still detected as long as the sedimentation motion accompanies velocity fluctuations due to the hydrodynamic perturbation or particle collisions in all the directions. In both geometries, the ultrasound pulses are repetitively captured to obtain a field matrix as shown in Scheme 1c. The field matrix contains two time axis components: the field time t and evolution time T. The temporal variation along the evolution time T contains the dynamic information on the microspheres. In order to evaluate the sedimentation velocity and its variance, the time correlation functions are calculated.

The ultrasound field correlation function is defined as

$$g^{(1)}(\tau) \equiv \frac{\langle \psi(t,T)\psi^*(t,T+\tau)\rangle}{\langle \psi(t,T)\psi^*(t,T)\rangle} = \langle \exp[-iq\cdot\Delta r(\tau)]\rangle \quad (2)$$

where Δr is the displacement of the microspheres during the time interval τ. The bracket indicates the evolution time average. Δr may be rewritten as a sum of the average displacement and the deviation from the average

$$\Delta r(\tau) = \langle \Delta r(\tau)\rangle + \delta r(\tau) \quad (3)$$

By substituting eq 3 into eq 2, one obtains

$$g^{(1)}(\tau) = \cos(q\langle \Delta r(\tau)\rangle) \exp\left(-\frac{1}{2}q^2\langle \delta r^2(\tau)\rangle\right) \quad (4)$$

Provided that the average displacement is zero in the case of diffusion process and the variance follows a Gaussian statistics with the well-known solution

$$\langle \delta r^2(\tau)\rangle = 2D\tau \quad (5)$$

eq 4 is reduced to the homodyne time-correlation function for the Brownian motion

$$g^{(1)}(\tau) = \exp(-Dq^2\tau) \quad (6)$$

where D is the translational diffusion coefficient of the scattered object. In the case of aqueous suspensions of microspheres studied here, sedimentation can dominate the dynamics because of the high Peclet number. However, the detectable information depends on the direction of the scattering vector with respect to the sedimentation direction. If the scattering vector is parallel (so is the beam direction) to the sedimentation direction, the average velocity along this direction and its fluctuations can be detected. Therefore, the sedimentation velocity, $\langle V_z\rangle$, and the velocity variance, $\langle \delta V_z^2\rangle$, are estimated from the following analysis. In this case, the time correlation function for the z-component is given by

$$g_z^{(1)}(\tau) = \cos(q\langle V_z\rangle\tau) \exp\left(-\frac{1}{2}q^2\langle \delta V_z^2\rangle\tau^2\right) \quad (7)$$

The particle diameter d may be obtained from the Stokes equation[28]

$$d = \sqrt{\frac{18\eta_0 V_0}{(\rho - \rho_0)g}} \quad (8)$$

where g is the acceleration gravity and V_0 is the terminal velocity, which may be obtained from extrapolating $\langle V_z\rangle$ to the zero concentration limit. V_0 may be expressed by the empirical Richardson−Zaki law[26]

$$V_0 = \frac{\langle V_z\rangle}{(1-\phi)^n} \quad (9)$$

where ϕ is the volume fraction and n is an exponent around 4.5−5.5 in the low Reynolds number regime. For sufficiently low concentration, V_0 may be expressed as[28]

$$V_0 = \frac{\langle V_z\rangle}{1 - 6.55\phi + O(\phi^2)} \quad (10)$$

On the other hand, when the incident beam is normal to the sedimentation direction, the time-correlation function contains only the velocity fluctuations since the scattering vector does not coincide with the sedimentation direction. For this particular case, the y-component of the correlation function can be expressed as

$$g_y^{(1)}(\tau) = \exp\left(-\frac{1}{2}q^2\langle \delta V_y^2\rangle\tau^2\right) \quad (11)$$

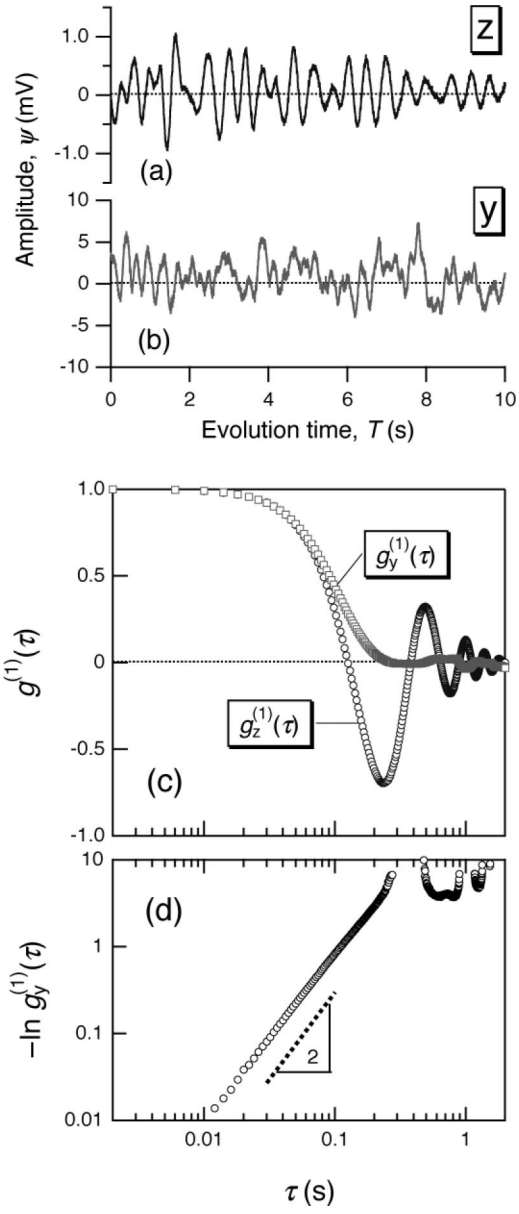

Figure 1. Examples of the field amplitude from (a) z- and (b) y-directions and (c) the corresponding $g^{(1)}(\tau)$. (d) A double-logarithmic plot of $-\ln g^{(1)}(\tau)$ vs τ revealing the τ-square dependence.

It should be noted that DSS provides the field correlation functions, $g^{(1)}(\tau)$, rather than the intensity correlation functions, $g^{(2)}(\tau)$, so that the dynamics can be evaluated without assuming field-to-intensity conversion, i.e., the so-called Siegert relation.[29] In addition, since a large number of correlation functions with the field time, t, as a variable are simultaneously obtained from a single acquisition, the information on the scattering path is always accessible for investigation of the strongly scattering systems.[21]

Figure 1a,b demonstrates typical amplitude fluctuations observed along the z- and y-directions. The corresponding correlation functions are exhibited in Figure 1c. The correlation functions were calculated by a FFT procedure (the correlation theorem[30]) and by a symmetrical normalization defined by eq 2. It is worth noting that the correlation functions obtained by this method have statistically high quality although they were obtained by software rather than by hardware like a photon correlator of light scattering systems. As demonstrated in Figure 1c, $g_z^{(1)}(\tau)$ exhibited negative overshoot because of the presence of the cosine term in eq 7. This is a characteristic feature of the nonzero average component attributed to sedimentation. On the other hand, $g_y^{(1)}(\tau)$ decayed rather monotonically as expected from eq 11. Figure 1d shows the relaxation time dependence of $-\ln g_y^{(1)}(\tau)$. Since $-\ln g_y^{(1)}(\tau)$ corresponds to the mean-square displacements and the slope found in the double-logarithmic plot is ≈2, it is concluded that DSS detects the particle motion obeying the above equations.

Figure 2 shows a series of time-correlation functions with different particle sizes $d = 3.6$, 5.5, 18, and 32 μm. For both (a) $g_z^{(1)}(\tau)$ and (b) $g_y^{(1)}(\tau)$, the larger particles exhibited more rapid decay. The solid lines are the results of fitting the data to eqs 7 and 11, respectively. As seen from the figure, the fitting was quite satisfactory, subsequently motivating us to carry out the evaluation of quantitative velocity.

Such correlation functions $g^{(1)}(\tau)$ were obtained as many as the points on the field-time axis from a single acquisition. Figure 3a,b shows two representative $g^{(1)}(\tau)$ images obtained for the 32 μm microspheres with $C = 1$ wt % observed from the z- and y-directions. Negative overshoot was found in all the field times in Figure 3a, whereas the monotonic decay was observed in Figure 3b. After carrying out nonlinear least-squares fit with eqs 7 and 11, the average sedimentation velocity $\langle V_z \rangle$ and the variances for z-direction $\langle \delta V_z^2 \rangle$ and y-direction $\langle \delta V_y^2 \rangle$ were evaluated. It was found that $\langle V_z \rangle$ and $\langle \delta V_z^2 \rangle^{1/2}$ had a weak dependence or rather invariant with respect to the field time, t. On the other hand, $\langle \delta V_y^2 \rangle^{1/2}$ exhibited a quadratic behavior as a function of t. These results will be discussed below.

Since $\langle V_z \rangle$ was irrespective of the field time, the obtained data were averaged, followed by conversion into the particle diameters $d_{DSS,z}$ ($= d$) using eqs 8 and 9. The density $\rho_0 = 0.9982$ g/cm^3 and viscosity $\eta_0 = 1.002$ cP for pure water at 20 °C were taken from refs 31 and 32. Figure 4 shows the concentration dependence of the evaluated diameters where the dashed lines represent the diameter obtained by SEM. After the concentration correction using the Richardson−Zaki equation, the corrected velocity was fairly close to the terminal velocity provided in Table 1, leading to the good agreement in the particle diameter between DSS and SEM results. Since the experiments were carried out at the fixed scattering angle, $\theta = 180°$, further experiments with various scattering angles will be a future task. In general, internal modes could also contribute to the dynamic scattering when $qa \approx 1$ with the particle radius a.

Let us discuss the variation of $\langle \delta V_y^2 \rangle^{1/2}$ with the field time found in Figure 3e. As described in the Introduction, DSS can probe the velocity fluctuations as a function of the field time. Figure 5 shows $\langle \delta V_y^2 \rangle^{1/2}$ obtained for the (a) 32 μm and (b) 5.5 μm microsphere suspensions in range $C = 0.5-2.9$ wt % as a function of the field time. Because it was a backscattering system, the scattering path x could be easily obtained from the product of the field time and ultrasound phase velocity v_p

$$x = \frac{v_p t}{2} \tag{12}$$

In the case of a single scattering system, x is connected to the sample position ($0 < x < 10$ mm) as shown in the top axis of the graphs.

When multiple scattering is observed, $g^{(1)}(\tau)$ decays more rapidly due to uncorrelated field for the longer path displacements, leading to the larger $\langle \delta V_y^2 \rangle^{1/2}$ with the longer field time.[21] On the other hand, if the particles interact with the cell wall, $\langle \delta V_y^2 \rangle^{1/2}$ will vary as well. For example, the Hagen−Poiseuille flow[33] could lead to a quadratic dependence of velocity on with the field time. For $d = 32$ μm, $\langle \delta V_y^2 \rangle^{1/2}$ increased with the field time in range $t < 5$ μs, as demonstrated in Figure 5a. At low concentrations, $\langle \delta V_y^2 \rangle^{1/2}$ seemed to level off at the larger t, followed by a decrease with t in range $8 < t < 14$ μs. However,

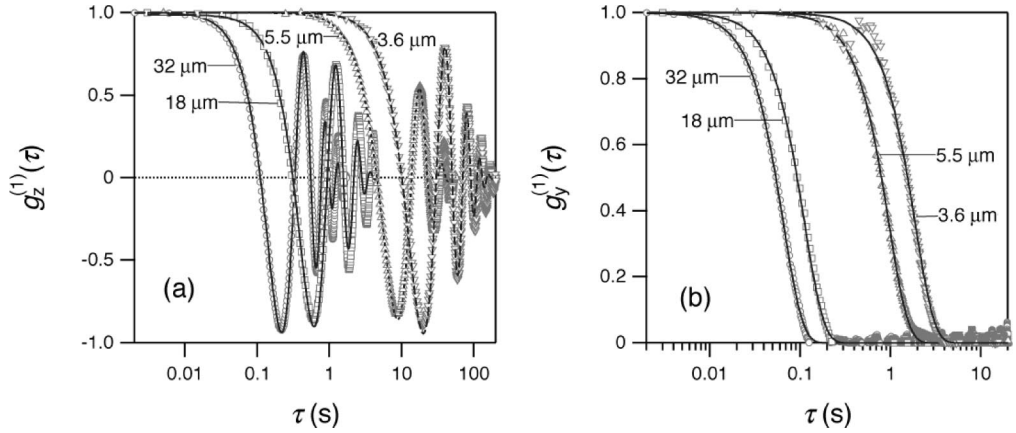

Figure 2. $g^{(1)}(\tau)$ of the microspheres with different particle diameters observed by the (a) vertical and (b) horizontal setups.

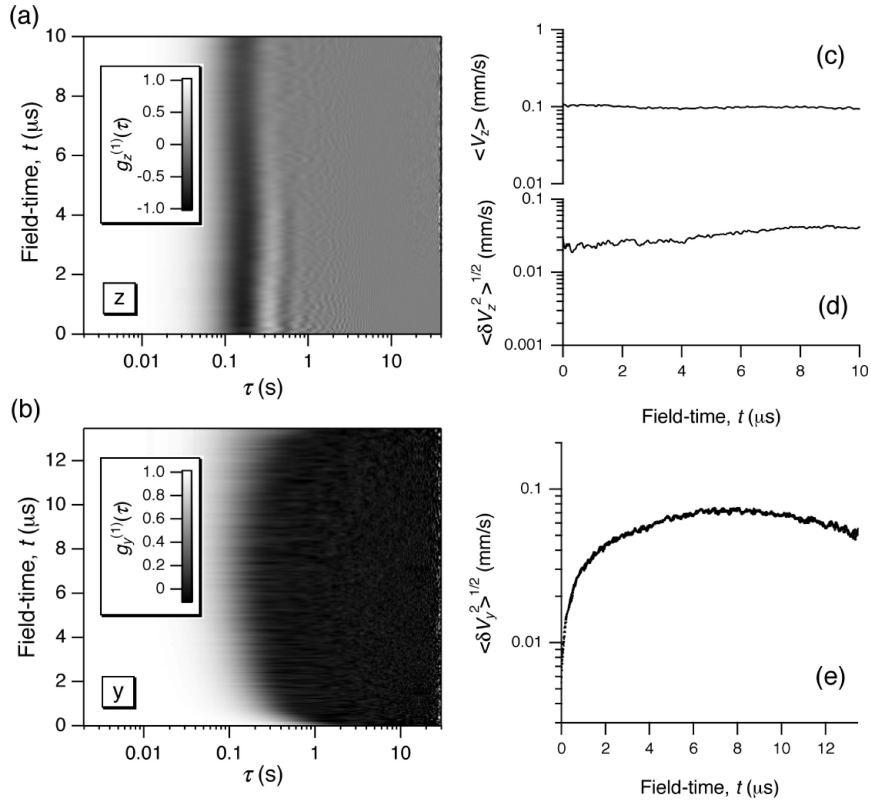

Figure 3. Two representative $g^{(1)}(\tau)$ images obtained for the 32 μm microspheres with $C = 2.9$ wt % observed from the (a) z- and (b) y-directions. Field-time dependences of (c) $\langle V_z \rangle$, (d) $\langle \delta V_z^2 \rangle^{1/2}$, and (e) $\langle \delta V_y^2 \rangle^{1/2}$.

as the concentration increases, the reduction of $\langle \delta V_y^2 \rangle^{1/2}$ for the larger t was unseen in the corresponding time region. Such an upturn was not observed for 5.5 μm microspheres; i.e., all the $\langle \delta V_y^2 \rangle^{1/2}$ vs t curve represented a quadratic behavior as shown in Figure 5b. From these experimental findings, it is deduced that the reduction of $\langle \delta V_y^2 \rangle^{1/2}$ may be due to a shear effect in sedimentation velocity or another wall effect on the velocity fluctuations. However, before arriving at the conclusion, one must consider the inherent behavior of wave scattering for the larger objects. Thus, the attenuation coefficient and the ultrasound velocity were systematically investigated with different particle sizes and concentrations as follows.

Figure 6 shows the frequency dependence of the attenuation coefficients α with different particle sizes obtained by the transmission setup. The particle concentration C was 2.9 wt %. α was estimated by the ratio of the Fourier magnitude $|\psi(f)|$ of the sample to the reference field pulses.[27]

$$\alpha(f) = -\frac{2}{L} \ln \frac{|\psi_{\text{sam}}(f)|}{|\psi_{\text{ref}}(f)|} \tag{13}$$

The number of scattering event can be estimated by[21]

$$n(t) = \frac{x(t)}{l^*} = \alpha v_g t \tag{14}$$

where $x = v_g t$ ($0 < x < 2L$ mm) is the wave propagation distance, v_g the group velocity, $l^* = 1/\alpha$ the scattering mean path, and $L = 10$ mm the cell width. In practice, the accurate L was determined by measuring echo pulses of pure water prior to the transmission experiments. If α is less than 0.05 mm^{-1} and v_g is not too different from that of the water, the detected signals

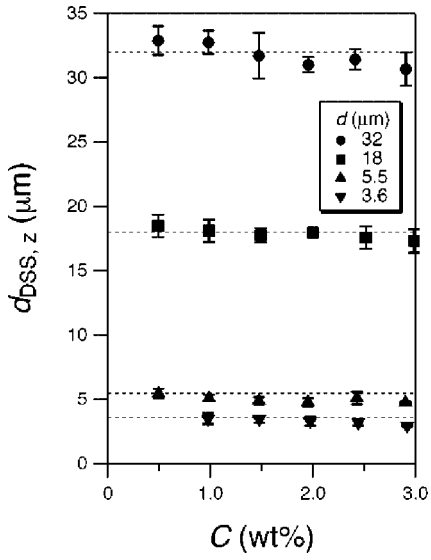

Figure 4. Concentration dependence of the particle diameter obtained by DSS.

can be always asserted to single scattering throughout the sample distance between two walls. As evidenced from the figure, this might be valid for $d = 3.6$ and 5.5 μm. However, the results for 18 and 32 μm exceed the acceptable limit for the single scattering approximation.

In order to investigate this problem further, the frequency dependence of the phase velocity v_p with the different particle sizes and concentrations were investigated. v_p can be obtained by[27]

$$v_p = \frac{2\pi Lf}{\Delta\Phi + 2\pi Lf/v_{water}} \quad (15)$$

where $\Delta\Phi$, L, and v_{water} (= 1.482 mm/μs) respectively are the phase difference between the sample and reference pulses, thickness of the sample, and ultrasound velocity of pure water,[34] which is known to be independent of f in this frequency range. As shown in Figure 7, v_p for the smaller particle sizes was invariant with respect to f for all the concentration ranges studied here. However, as the particle size became larger, v_p exhibited a strong frequency dependence as well as resonance scattering,[35−37] which was attributed to the coincidence with the frequencies of the free-body (i.e., in a vacuum) vibration modes. However, the f dependence of v_p seemed to be less important for the lower concentration even in the larger particle size. An extensive study concerning the α and v_p by using the dispersion relation[38] can be found in the literature.[39] Apart from the large scatterers, one could find extensive literatures describing acoustic scattering for small particles.[40−44] Note that the thermal and viscous waves inherent in acoustic scattering were of importance for the long wavelength limit (for small particles) and believed to be insignificant for the micron-size particles where the resonance scattering played the most important role.[45,46]

From the findings, we reached the following conclusions. First, the symmetry of the velocity fluctuations $\langle \delta V_y^2 \rangle^{1/2}$ was confirmed for $d = 3.6$ and 5.5 μm, while a decrease in $\langle \delta V_y^2 \rangle^{1/2}$ near the two cell walls was observed. Therefore, the t-independent region was extracted and averaged to evaluate sufficient quality of $\langle \delta V_y^2 \rangle^{1/2}$ in the subsequent analysis. Second, an upturn in $\langle \delta V_y^2 \rangle^{1/2}$ for $d = 18$ and 32 μm at the high concentration was observed although $\langle \delta V_y^2 \rangle^{1/2}$ followed the similar behavior at the front wall ($t < 5$ μs). The origin of the asymmetry of $\langle \delta V_y^2 \rangle^{1/2}$ may be explained as follows: Most of the particles will scatter only one time if α is negligibly small. It leads to an idea that the field time t can be reread to the sample position between the two walls by multiplying v_p. However, the scattering loss α becomes more significant for the larger particles, indicating that the hypothesis is no longer valid particularly for the longer field time, i.e., the larger scattering path. When multiple scattering occurs, the corresponding field becomes uncorrelated, resulting in more rapid decay in $g^{(1)}(\tau)$. This could account for the origin of the asymmetry of the horizontal fluctuations observed in Figure 5a.

Finally, the concentration dependence of $\langle \delta V_y^2 \rangle^{1/2}$ with different particle sizes is exhibited in Figure 8a. As explained above, $\langle \delta V_y^2 \rangle^{1/2}$ obtained by the correlation function analysis was further averaged over the field-time region, which was free from the wall effect. While the average velocity is well

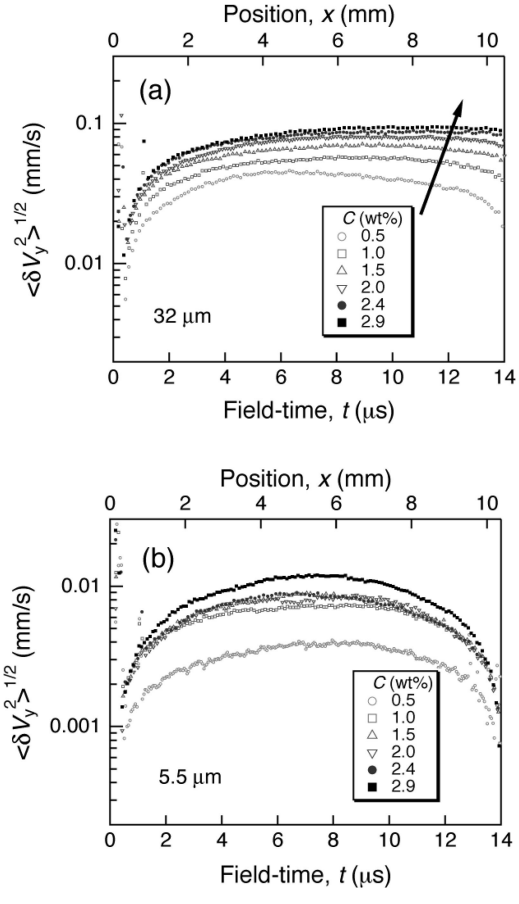

Figure 5. Field-time dependences of $\langle \delta V_y^2 \rangle^{1/2}$ obtained for the (a) 32 μm and (b) 5.5 μm microsphere suspensions in range $C = 0.5-2.9$ wt %.

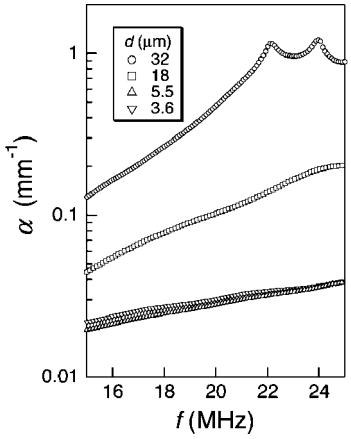

Figure 6. Frequency dependence of the attenuation coefficient α with different particle sizes.

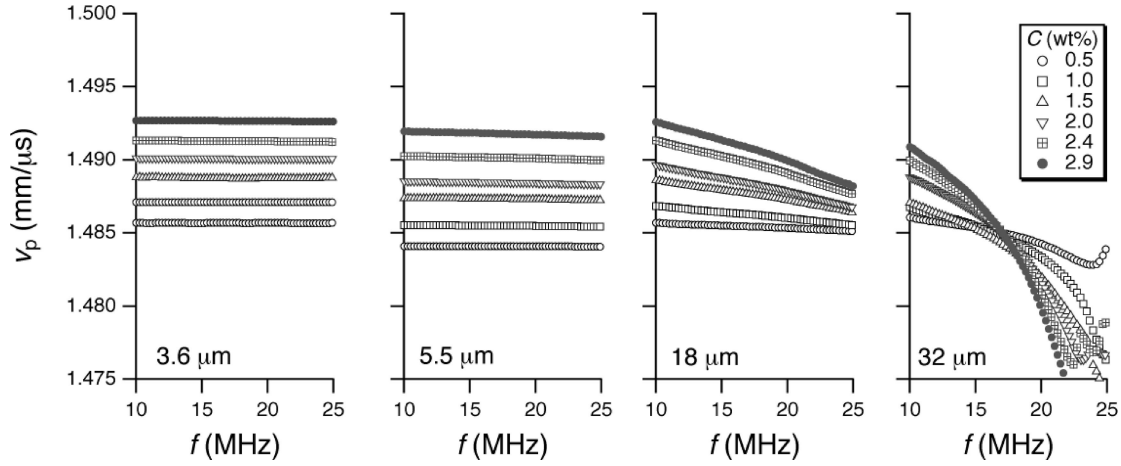

Figure 7. Frequency dependence of v_p with different particle sizes and concentrations.

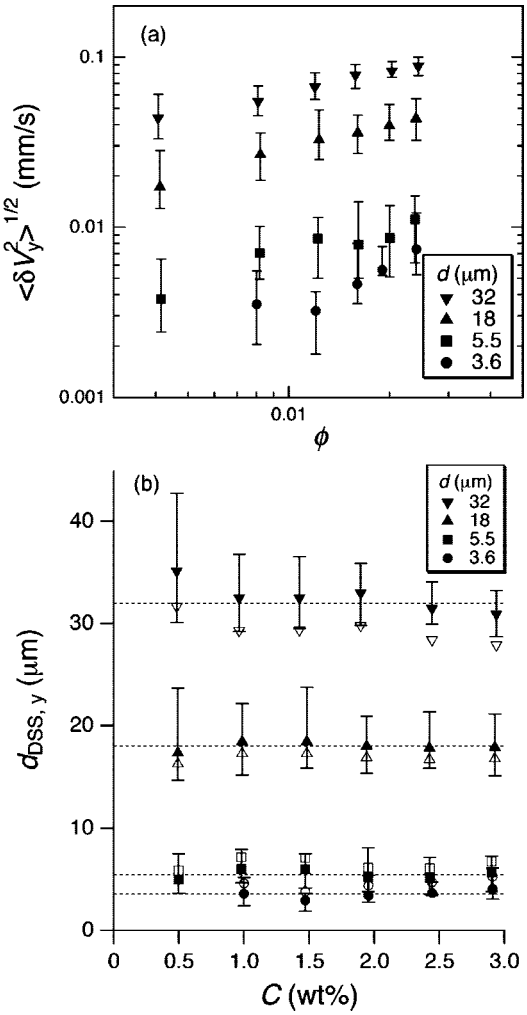

Figure 8. (a) Plot of $\langle \delta V_y^2 \rangle^{1/2}$ vs ϕ obtained for different particle sizes. (b) Particle diameter calculated by eq 17. The solid and open symbols respectively indicate the results with the size-dependent and -independent C_y (see text). The dashed lines indicated the values obtained by SEM.

understood,[28] the velocity fluctuations still remain the matter of interest in the field of fluid dynamics because of their complexity and versatility in the dynamic aspects.[47−49] When the interface (between clear water and suspended particle phase) is formed during sedimentation, two antagonistic behaviors, broadening and self-sharpening of the interface, simultaneously take place.[47,50−53] The polydispersity leads to the former behavior because the larger particle sediments more rapidly than the smaller one. Note that such a broadening occurs even if the particles are monodisperse owing to hydrodynamics interactions. On the contrary, self-sharpening that competes with the broadening of the interface also takes place. The self-sharpening of the interface occurs because the concentrated particles settled earlier are overtaken in the upper phase consisting of the lower concentration phase (since the particles in more dilute phase settle faster). However, such a broadening effect is believed to be less important for the higher concentration due to the appearance of the hindered settling, i.e., back-flow of the particles from the bottom.[28] In any case, all the effects could contribute more or less to the velocity fluctuations $\langle \delta V_y^2 \rangle^{1/2}$ investigated in this study. It is also noted that the velocity fluctuations are system size dependent; i.e., it is strongly influenced not only by the above-mentioned phenomena but also by the cell size.[54−56] Dynamic structures originated from the long-range hydrodynamic fluctuations[57] are still the matter of scientific interest.

Besides the delicate balance of the hydrodynamics interactions, density fluctuations obeying Poisson statistics are considered to be one of the main causes of the velocity fluctuations. Then the velocity fluctuations can be obtained by balancing the buoyant mass force with the Stokes drag[58−60]

$$\langle \delta V_y^2 \rangle^{1/2} = C_y V_0 \sqrt{\frac{2\phi L}{d}} \tag{16}$$

where V_0, ϕ, L, d, and C_y respectively are the terminal velocity, volume fraction of the microsphere, sample thickness, particle diameter, and a proportional constant. While the constant is $(3/4\pi)^{1/2}$ in the simplest case, various C_y were reported depending on the direction and cell size.[54] Subsequently, the particle size evaluation was attempted by using the model. After substituting the relation of the Stokes velocity eq 8 into eq 16, one may obtain the particle diameter ($d_{DSS,y} = d$)

$$d_{DSS,y} = \left(\frac{18\eta_0 \langle \delta V_y^2 \rangle^{1/2}}{C_y(\rho - \rho_0)g} \right)^{2/3} (2\phi L)^{-1/3} \tag{17}$$

Figure 8b shows $d_{DSS,y}$ calculated by eq 17 with different concentrations. It is worthwhile to note that there is no adjustable parameter to obtained the results except the proportional constant $C_y = 0.28$ (open symbols).[54] The dashed lines indicated the particle diameter d obtained by SEM. If one assumes C_y being particle size dependent, the best fit provided $C_y = 0.408$, 0.362, 0.254, and 0.24 respectively for $d = 3.6$, 5.5, 18, and 32 μm as demonstrated by the solid symbols in Figure 8b. Although

estimation of the particle size from the velocity fluctuations was a tentative attempt, it was rather surprising that the particle size could be estimated from *y*-direction where no average component related to sedimentation was employed. Since the velocity fluctuations are extremely sensitive to the cell size, direction, and other factors, further investigation will be required to achieve more precise analysis from the horizontal setup.

Conclusions

Dynamic ultrasound scattering with 20 MHz longitudinal waves was developed in order to investigate dynamics of polymer microspheres in highly turbid suspensions. Two types of experimental setup were employed to evaluate the average velocity and its fluctuations along the directions parallel (z) and perpendicular (y) to the sedimentation direction. From the z-direction, the field correlation functions allowed estimation of the average sedimentation velocity, thereby particle sizing via the Stokes equation. On the other hand, the velocity fluctuations were solely determined from the y-direction experiments. The particle sizes were also evaluated from the velocity fluctuations with the aid of a model proposed in the literature. Another advantage of using DSS may be that the position-dependent information from each field data can be acquired from a single measurement. The velocity fluctuations were obtained as a function of the distance from the wall of the sample cells. Particularly, the velocity fluctuations exhibited pronounced reduction near the cell walls. While the parabolic behavior is well-known as the Hagen−Poiseuille flow, the velocity fluctuations are also affected by the number of particles which would be different in the region close to the wall and at the center of the cell. Although the resonance scattering could contribute to the dynamics, it was affected only by the larger particles at the higher concentrations.

Acknowledgment. This work was supported by Grant-in-Aid No. 20750178 and Grant-in-Aid for Scientific Research on Priority Area, "Soft Matter Physics" (No. 463/19031018), from the Ministry of Education, Science, Sports, Culture, and Technology.

References and Notes

(1) *Characterization and Analysis of Polymers*; Wiley-Interscience: New York, 2008.
(2) Raffel, M.; Willert, C. E.; Wereley, S. T.; Kompenhans, J. *Particle Image Velocimetry*; Springer: Berlin, 2007.
(3) Evans, D. H. *Doppler Ultrasound: Physics, Instrumentation, and Clinical Applications*; Wiley: New York, 2000.
(4) Berne, B. J.; Pecora, R. *Dynamic Light Scattering with Applications to Chemistry, Biology and Physics*; Dover Publications: Mineola, NY, 2000.
(5) Li, J.; Li, W.; Huo, H.; Luo, S.; Wu, C. *Macromolecules* **2008**, *41*, 901.
(6) Stepanek, P.; Tuzar, Z.; Kadlec, P.; Krýz, J. *Macromolecules* **2007**, *40*, 2165.
(7) Kanao, M.; Matsuda, Y.; Sato, T. *Macromolecules* **2003**, *36*, 2093.
(8) Konak, C.; Helmstedt, M.; Bansil, R. *Polymer* **2000**, *41*, 9311.
(9) Hecht, A.-M.; Horkay, F.; Schleger, P.; Geissler, E. *Macromolecules* **2002**, *35*, 8552.
(10) Norisuye, T.; Tran-Cong-Miyata, Q.; Shibayama, M. *Macromolecules* **2004**, *37*, 2994.
(11) Norisuye, T.; Morinaga, T.; Tran-Cong-Miyata, Q.; Goto, A.; Fukuda, T.; Shibayama, M. *Polymer* **2005**, *46*, 1982.
(12) Osa, M.; Abe, F.; Yoshizaki, T.; Einaga, Y.; Yamakawa, H. *Macromolecules* **1996**, *29*, 2302.
(13) Willand, S.; Leipertz, A. *Int. J. Thermophys.* **2001**, *22*, 317.
(14) Fröba, A. P.; Willand, S.; Leipertz, A. *Int. J. Thermophys.* **2000**, *21*, 603.
(15) Cowan, M. L.; Page, J. H.; Weitz, D. A. *Acoust. Imaging* **2002**, *26*, 247.
(16) Cowan, M. L.; Page, J. H.; Weitz, D. A. *Phys. Rev. Lett.* **2000**, *85*, 453.
(17) Strybulevych, A.; Leary, D. M.; Page, J. H. *AIP Conf. Proc.* **2004**, *708*, 444.
(18) Strybulevych, A.; Page, J. H. *Microgravity Sci. Technol.* **2005**, *16*, 249.
(19) Strybulevych, A.; Norisuye, T.; Hasselfield, M.; Page, J. H. *AIP Conf. Proc.* **2008**, *982*, 354.
(20) Kohyama, M.; Norisuye, T.; Tran-Cong-Miyata, Q. *Polym. J.* **2008**, *40*, 398.
(21) Cowan, M. L.; Jones, I. P.; Page, J. H.; Weitz, D. A. *Phys. Rev. E* **2002**, *65*, 0666605.
(22) Galinsky, G.; Burchard, W. *Macromolecules* **1997**, *30*, 6966.
(23) Takata, Y.; Norisuye, T.; Hirayama, S.; Takemori, T.; Tran-Cong-Miyata, Q.; Nomura, S. *Macromolecules* **2007**, *40*, 3773.
(24) Morse, P. M.; Ingard, K. U. *Theoretical Acoustics*; Princeton University Press: Princeton, NJ, 1987.
(25) Shung, K. K.; Thieme, G. A. *Ultrasonic Scattering in Biological Tissues*; CRC: Boca Raton, FL, 1993.
(26) Richardson, J. F.; Zaki, W. N. *Chem. Eng. Res. Des.* **1954**, *32*, 35.
(27) Norisuye, T.; Strybulevych, A.; Scanlon, M.; Page, J. H. *Macromol. Symp.* **2006**, *242*, 208.
(28) Batchelor, G. K. *J. Fluid Mech.* **1972**, *52*, 245.
(29) Siegert, A. J. F. MIT Radiation Lab. Report No. 465, **1943**.
(30) Press, W. H.; Teukolsky, S. A.; Vetterling, W. T.; Flannery, B. P. *Numerical Recipes*; Cambridge University Press: Cambridge, 1992.
(31) Kell, G. S. *J. Chem. Eng. Data* **1975**, *20*, 97.
(32) Cho, C. H. *J. Phys. Chem. B* **1999**, *103*, 1991.
(33) Zheng, H. R.; Liu, L. L.; Williams, L.; Hertzberg, J. R.; Lanning, C.; Shandas, R. *Appl. Phys. Lett.* **2006**, *88*, 261915.
(34) Marczak, W. *J. Acoust. Soc. Am.* **1997**, *102*, 2776.
(35) Faran, J. J. *J. Acoust. Soc. Am.* **1951**, *23*, 405.
(36) Hay, A. E.; Schaafsma, A. S. *J. Acoust. Soc. Am.* **1989**, *85*, 1124.
(37) Brill, D.; Gaunaurd, G. *J. Acoust. Soc. Am.* **1987**, *81*, 1.
(38) Waterman, P. C. *J. Math. Phys.* **1961**, *2*, 512.
(39) Mobley, J.; Waters, R. K.; Hall, S. C.; Marsh, N. J.; Hughes, S. H.; Brandenburger, H. G.; Miller, G. J. *J. Acoust. Soc. Am.* **1999**, *106*, 652.
(40) Epstein, P.; Carhart, R. R. *J. Acoust. Soc. Am.* **1953**, *25*, 553.
(41) Allegra, J. R.; Hawley, S. A. *J. Acoust. Soc. Am.* **1972**, *51*, 1545.
(42) Challis, R. E.; Tebbutt, J. S.; Holmes, A. K. *J. Phys. D* **1998**, *31*, 3481.
(43) Challis, R. E.; Povey, M. J. W.; Mather, M. L.; Holmes, A. K. *Rep. Prog. Phys.* **2005**, *68*, 1541.
(44) McClements, D. J. *J. Acoust. Soc. Am.* **1999**, *105*, 915.
(45) Richter, A.; Babick, F.; Ripperger, S. *J. Acoust. Soc. Am.* **2005**, *118*, 1394.
(46) Richter, A.; Babick, F.; Ripperger, S. *Ultrasonics* **2006**, *44*, e483.
(47) Gomez, D. C.; Bergougnoux, L.; Guazzelli, E.; Hinch, J. *Phys. Fluids* **2008**, *20*, 023302.
(48) Gomez, D. C.; Bergougnoux, L.; Hinch, J.; Guazzelli, E. *Phys. Fluids* **2007**, *19*, 098102.
(49) Tee, S. Y.; Mucha, P. J.; Brenner, M. P.; Weitz, D. A. *Phys. Fluids* **2007**, *19*, 113304.
(50) Mucha, P. J.; Brenner, M. P. *Phys. Fluids* **2003**, *15*, 1305.
(51) Bergougnoux, L.; Ghicini, S.; Guazzelli, E. *Phys. Fluids* **2003**, *15*, 1875.
(52) Martin, J.; Rakotomalala, N.; Salin, D. *Phys. Fluids* **1994**, *6*, 3215.
(53) Lee, S. *Phys. Fluids* **1992**, *4*, 2601.
(54) Mucha, P. J.; Tee, S. Y.; Weitz, D. A.; Shraiman, B. I.; Brenner, M. P. *J. Fluid Mech.* **2004**, *501*, 71.
(55) Ladd, A. J. C. *Phys. Rev. Lett.* **2002**, *28*, 048301.
(56) Tee, S. Y.; Mucha, P. J.; Cipelletti, L.; Manley, S.; Brenner, M. P.; Segre, P. N.; Weitz, D. A. *Phys. Rev. Lett.* **2002**, *89*, 054501.
(57) Segre, P. N. *Phys. Rev. Lett.* **1997**, *79*, 2574.
(58) Brenner, M. P. *Phys. Fluids* **1999**, *11*, 754.
(59) Caflisch, R. E.; Luke, J. H. C. *Phys. Fluids* **1985**, *28*, 759.
(60) Hinch, E. J. In *Sedimentation of Small Particles in Disorder and Mixing*; Guyon, E., Nadal, J.-P., Pomeau, Y., Eds.; NATO ASI E; Kluwer Academic: Dordrecht, 1988; Chapter IX, p 153.

MA801949Y